Journal of Membrane Science 661 (2022) 120855

Contents lists available at ScienceDirect

Journal of Membrane Science

journal homepage: www.elsevier.com/locate/memsci

Tuning the surface functionality of polyamide films via termination reaction in molecular layer-by-layer deposition

Christopher M. Stafford [a,**,1], Xun Guan [b,1], Yarong Qi [b,2], Yue Zhang [c], Xitong Liu [b,*]

[a] Materials Science and Engineering Division, National Institute of Standards and Technology, Gaithersburg, MD, 20899, United States
[b] Department of Civil & Environmental Engineering, The George Washington University, 800 22nd St NW, Washington D.C., 20052, United States
[c] Department of Environmental Health and Engineering, Johns Hopkins University, Baltimore, MD, 21218, United States

ARTICLE INFO

Keywords:
Polyamide
Molecular layer-by-layer deposition
Fouling
Atomic force spectroscopy
Surface chemistry

ABSTRACT

Molecular layer-by-layer (mLbL) deposition of highly crosslinked polyamide-based membranes affords flexibility and control over membrane properties such as thickness, roughness, and chemistry of the selective membrane layer. Of particular interest is the ability to non-destructively tailor the surface chemistry of the membrane for a particular purpose, such as enhancing hydrophilicity or minimizing membrane fouling. Here, we show that the surface chemistry of the mLbL membrane can be tuned via termination reactions to render the surface rich in –COOH, $-NH_2$, −polyethylene glycol (−PEG), or −fluorinated groups. We systematically characterize the resulting surfaces with X-ray photoelectron spectroscopy (XPS) and atomic force microscopy (AFM) to validate successful modification and to ensure the low surface roughness is maintained, respectively. We then use pH-dependent contact angle and carboxylate-modified colloidal probe AFM to measure the surface wettability and adhesion of the modified surfaces. The measured adhesion force follows the ranking $-NH_2 \gg$ −fluorinated > –COOH ≈ −PEG, where the –COOH and −PEG are repulsive due to charge interactions and hydration state, respectively. Combined with the low surface roughness afforded by mLbL deposition, surface functionalization through termination reactions as shown here will allow researchers to disentangle contributions of surface chemistry from surface roughness to the overall performance and fouling of polyamide-based membranes for water purification and advanced chemical separations.

1. Introduction

To tackle the grand challenge of water scarcity, membrane-based reverse osmosis (RO) technology plays an important role in harvesting freshwater from unconventional water sources such as brackish water, seawater, and wastewater [1–4]. The state-of-the-art commercial RO membranes are thin-film composite polyamide membranes first invented by Cadotte and co-workers in the late 1970s [5,6]. These membranes are prepared via interfacial polymerization (IP) of an acid chloride (e.g., trimesoyl chloride, TMC, dissolved in an organic solvent) and a diamine (e.g., *m*-phenylenediamine, MPD, dissolved in water) atop a polymeric porous support (e.g., a polysulfone membrane) [7]. Despite their excellent water permeability and salt rejection [7], the IP membranes have a ridge-and-valley structure with a high roughness as well as a non-uniform distribution of polar functional groups [8,9], because of the rapid, uncontrolled polymerization reaction at the organic-water interface. The high roughness and heterogeneity of IP polyamide membranes not only contribute to a high propensity to undergo organic and colloidal fouling [10,11], but also impede fundamental understandings of structure-property relationships of the membranes [12].

To overcome the limitations of IP polyamide, molecular layer-by-layer (mLbL) deposition has been developed to enable the fabrication of polyamide membranes in a well-controlled manner [12–15]. In mLbL deposition, the polyamide films are built one monomer layer at a time by sequential reaction of an acid chloride and a diamine, both dissolved in an organic solvent [12,13]. The mLbL deposited polyamide membranes have shown improved water permeability and salt rejection than the commercial IP polyamide membranes [14,15]. In addition, the mLbL

* Corresponding author.
** Corresponding author.
E-mail addresses: chris.stafford@nist.gov (C.M. Stafford), xitongliu@gwu.edu (X. Liu).
[1] Both authors contributed equally to this work.
[2] Present address: Department of Environmental Science, Policy, and Management, University of California, Berkeley, CA, 94,720, United States.

https://doi.org/10.1016/j.memsci.2022.120855
Received 18 April 2022; Received in revised form 15 July 2022; Accepted 20 July 2022
Available online 10 August 2022

polyamide membranes possess additional advantages of minimum roughness, precisely controlled thickness, and well-defined polymer chemistry [14]. Thus, mLbL synthesis of polyamides has proven to be a unique platform that allows elucidation of the fundamental relationships between polymer network structure, membrane thickness, and separation performance [16–19].

Another important attribute of the mLbL technique is the ability to precisely control the terminating functional groups on the deposited polyamide film [20]. Surface properties of membranes dictate their interaction with foulants, which, in turn, determine the fouling behaviors of the membranes in complex waters [21]. For example, the density of carboxyl groups on polyamide has been related to the propensity for the membrane to undergo alginate fouling in the presence of calcium ions [22]. In addition, while increasing hydrophilicity of membranes is generally effective for reducing the adhesion of foulants, the inclusion of low-surface-energy hydrophobic perfluoroalkyl groups can lead to enhanced fouling release [23]. An intriguing research question emerges: is it possible to use the mLbL technique to fabricate polyamide films with a wide range of terminating functional groups, including those that have varied hydrophilicity?

In this study, we employed the mLbL deposition technique to fabricate polyamide films on silicon substrates. We reacted the as-cast polyamide with different terminating functional groups, including TMC, MPD, hydrophilic polyethylene glycol (PEG)-amine, and hydrophobic perfluoroalkyl amine. We systematically characterized the thickness, surface functionality, and roughness of the polyamide films using ellipsometry, X-ray photoelectron spectroscopy (XPS), and atomic force microscopy (AFM) imaging, respectively. We further characterized the surface wetting property and ionization behaviors of the polyamide surfaces using buffered contact angle titration. Finally, we employed AFM to determine the interaction forces between the polyamide surfaces and a carboxylate-modified latex colloid probe. Our results demonstrate that reacting the as-cast polyamide surface with different monomers allows control over the surface functionality and hydrophilicity of the polyamide, as well as the interaction with the colloid probe. Our work highlights the versatility of the mLbL technique in fabricating polyamide membranes with well-controlled surface chemistry and paves the way for further investigations into the structure-property relationships of polyamide membranes.

2. Experimental

2.1. Materials

Equipment and materials are identified in the article to adequately specify the experimental details. Such identification does not imply recommendation by the National Institute of Standards and Technology, nor does it imply that the materials are necessarily the best available for the purpose.

Trimesoyl chloride (TMC), *m*-phenylenediamine (MPD), and poly (ethylene glycol) bis(amine) (PEG-NH_2, number average relative molecular mass of 3400) were purchased from Sigma Aldrich and used as received. 1H,1H-Perfluorooctylamine was purchased from Alfa Aesar and used as received. 3-Aminopropyldimethylethoxysilane (APDES) was purchased from Gelest and used as received. Toluene, ethanol, and acetone were purchased from Fisher Scientific. Toluene was dried over 3 Å molecular sieves and had a water content of less than 10 ppm (10 mg/kg) as measured on a Karl Fischer CS20X coulometric titrator (Mettler Toledo). Acetone was dried and purified via vacuum distillation into a sealed Schlenk round bottom flask and kept under constant nitrogen purge. Prior to vacuum distillation, acetone (700 mL) was stirred over potassium carbonate (300 g) overnight.

Silicon wafers (orientation <100>, University Wafers, 1.5 cm × 1.5 cm) were cleaned by rinsing with toluene and ethanol, dried with nitrogen, then treated with ultraviolet-ozone (Model 342, Jelight) for 20 min. To ensure covalent attachment of the mLbL polyamide films to the substrate, the silicon wafers were treated with an aminosilane prior to mLbL deposition. The cleaned silicon wafers were submerged in a solution of 1% by mass fraction of APDES in dry toluene and gently heated at 50 °C for 12 h. The APDES-modified silicon wafers were then rinsed with toluene, ethanol, deionized water (18 MΩ/cm, Barnstead Nanopure) and dried in a vacuum oven for 24 h.

2.2. mLbL polyamide film preparation

mLbL polyamide films were prepared according to previous literature [16,24]. Monomer solutions were prepared at 0.4% by mass fraction of TMC in toluene and 0.4% by mass fraction of MPD in toluene. The rinse solvent following TMC deposition was toluene, and the rinse solvent following MPD deposition was acetone. Solutions/rinse solvents were loaded into gas-tight syringes and deposited through 0.45 μm syringe filters onto the APDES-modified silicon substrate inside an environmental spin coater (Laurell Technologies) purged with clean, dry air to minimize exposure to water [24]. One deposition cycle consisted of the sequential deposition and spinning of TMC (0.4 mL), toluene rinse (0.8 mL), MPD (0.4 mL), and acetone rinse (0.8 mL) at room temperature. The thickness of the mLbL polyamide was controlled by the number of deposition cycles, which in all cases presented here was 45.5 cycles. The final half cycle ensured that the mLbL polyamide film presented predominantly acid chloride groups at the surface for subsequent reaction with the amine reagents. The samples were prepared in triplicate for each surface functionalization.

2.3. mLbL surface functionalization

After mLbL deposition, each sample was cleaved such that a section of the sample was retained for measurements of "before" functionalization (control), and the remainder of the sample was functionalized with the specific reagent and measured "after" functionalization. For functionalization, the reagent of choice was dissolved at a concentration of 1% mass fraction in dry toluene and heated to 75 °C. The mLbL polyamide film was then immersed in the solution and the reaction was allowed to proceed for 48 h to ensure maximum functionalization. It should be noted that we chose a difunctional PEG-amine (amine groups on either end of the PEG chain) to ensure the PEG chains adequately react to the surface and form loops of PEG chains rather than a brush-like PEG structure. The samples were then rinsed twice each with toluene, ethanol, water, and finally with ethanol again, then dried with nitrogen. The control samples were immersed in dry toluene (no reagent), heated to 75 °C for 48 h, and rinsed using the same protocols as above.

2.4. mLbL polyamide film characterization

Each polyamide sample was characterized both before and after functionalization. The thickness of the mLbL polyamide films was characterized via variable angle spectroscopic ellipsometry (M-2000XI, J.A. Woollam). Spectra were obtained at incidence angles in the range of 50°–70° in discrete increments of 10° and over a wavelength range of (210–1700) nm. The film thickness was modelled assuming a Cauchy dispersion relation using the CompleteEASE software provided by J.A. Woollam. Chemical functionalization was confirmed by X-ray photoelectron spectroscopy (XPS, AXIS Ultra DLD Spectrometer, Kratos Analytical). XPS measurements were performed using a monochromatic Al K_α source (1486.6 eV) operating at 140 W. The base pressure of the sample analysis chamber was $\approx 1.0 \times 10^{9}$ Torr (or 1.33×10^{7} Pa), and spectra were collected from a nominal spot size of 300 μm × 700 μm and a take-off angle of 90° (normal to the surface). Measurements were performed in hybrid mode using electrostatic and magnetic lenses, and the pass energy of the analyzer was set at 160 eV for survey scans and 20 eV for high resolution scans, with energy resolutions of 0.5 eV and 0.1 eV, respectively. All XPS data analysis and peak fitting were performed using the CasaXPS software package.

2.5. Buffered contact angle titration

Buffered contact angle titration was performed on a goniometer (ramé-hart 260-U4) via the sessile drop method. The sample films (control, MPD, TMC, PEG-NH_2, and perfluorooctyl amine) were rinsed with ethanol and ultrapure water, and dried with ultrapure N_2 gas prior to the contact angle measurement and in between different measurements. A 1-μL droplet of buffered aqueous solution was placed on the sample using a pipette. For all film types, the droplet was allowed to stay on the surface for between a few seconds and 1 min, in order to reach a steady solution-surface interface and also to avoid complete water evaporation from the droplet. Buffer solutions of pH ranging from 2 to 10 that contain 1 mol/L of buffer chemicals [20,25] (see Table S1) were used for the measurement. The static contact angle was determined by measuring the tangent angle of the liquid drop at the point of contact after the liquid-surface interface came to equilibrium. Three contact angle measurements were performed at each pH.

2.6. AFM imaging and interaction force measurement

We conducted AFM imaging of the polyamide films on a Multimode 8 AFM (Bruker). Prior to the imaging, the samples were rinsed with ethanol to remove possible contaminants and dried with ultrapure N_2. A ScanAsyst-Air probe (Bruker) was used for the imaging. The root-mean-square (rms) roughness of the films was determined from three measurements at different locations.

We conducted force measurement between a carboxylate-modified latex (CML) probe and the polyamide films in aqueous solutions. The CML particle serves as a surrogate for organic foulants that are rich in carboxylic acid groups (such as humic acid and proteins) and has been used extensively for characterizing foulant-surface interactions [26,27]. A CML sphere with a diameter of 10 μm (Molecular Probes Latex Beads, 4% w/v) was glued to the D cantilever of an NP-O10 probe (Bruker). The CML-modified probe was cleaned using ultrapure water and subjected to UV/Ozone treatment (UV-Ozone ProCleaner Plus, Nanosciences) for 10 min to remove possible organic contaminants on the probe. The spring constant of the cantilever after CML modification was measured using the thermal noise method [28]. Before force measurement, the probe was rinsed with a buffer (1 mmol/L NaCl and 0.2 mmol/L $NaHCO_3$, pH 7.5). During force measurement, a droplet of buffer solution (1 mmol/L NaCl and 0.2 mmol/L $NaHCO_3$, pH 7.5) was placed in a fluid cell and allowed to equilibrate with the polyamide films for at least 30 min. With the buffer, the Debye length is 8.8 nm which accentuates the differences in electrical double layer forces with regard to the different surface chemistries. The probe was brought to the sample surface at a constant approach velocity of 500 nm/s, with a trigger threshold of 200 nm and 1 s dwell time at the surface. The probe was then retracted from the sample surface at a velocity of 500 nm/s. The ramp size was 1000 nm. For each sample, force curves were measured at 256 locations in an area with a scan size of 10 μm. In between force measurements on different surfaces, the probe was rinsed with ethanol and DI water, but not subjected to UV-ozone cleaning to avoid further change in the probe surface chemistry.

The raw AFM force data of deflection vs displacement were analyzed using a published software [29] (https://github.com/spacocha/fdafm). In short, the deflection-displacement raw data were converted into interaction force-separation distance curves using previously reported methods [30,31], from which maximum adhesive force, adhesive interaction energy (i.e., area above the force-distance curve and under the *x*-axis), and repulsive interaction energy (i.e., area under the force-distance curve and above the *x*-axis) were calculated. This method of obtaining interaction energy via integration of force curves has been extensively used in previous publications [26,27,32,33]. For each retract force curve, we also calculated the total interaction energy, by adding up the repulsive and attractive interaction energies, based on previously reported approach [27,32]. The total interaction energy here represents the work required to pull the probe away from the surface after contact [27,34]. To stay consistent with the sign convention of interaction force and aid data interpretation, we denote adhesive and repulsive total interaction energy as negative and positive, respectively. To further compare the interaction characteristics between CML probe and the polyamide films, we analyzed repulsive distance (i.e., the distance between contact point and the location where repulsive force becomes zero) and rupture length (i.e., the distance between contact point and the location where adhesive force becomes zero) of the corresponding retract force curves. We randomly select 50 force curves out of 256 curves after removing the outliers using the Grubbs' test (significance level 0.05, https://www.graphpad.com/quickcalcs/grubbs1/), and present the descriptive statistics of the data (e.g., adhesive force, total interaction energy) in Figs. 5–7.

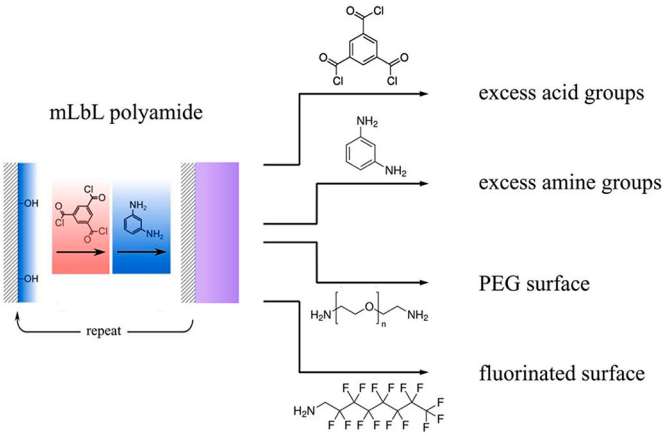

Fig. 1. Process for creating mLbL films via repetitive reaction of the substrate with TMC and MPD, rinsing away unreacted monomers between each reaction step. The thickness of the film is determined by the total number of repetition cycles performed (here, 45.5 cycles). The surface of the mLbL film is then reacted with various reagents to create the desired surface functionality.

Table 1
Thickness data for each sample series before and after functionalization with the specific reagent. The error bars represent one standard deviation of the data (n = 9, measurements at three random locations on each of the three replicate samples), which is taken as the experimental uncertainty of the measurement.

Reagent	thickness (nm)		
	as-cast	after reaction	*p-value (paired t-test)*
TMC	17.9 ± 3.0	16.1 ± 1.1	0.09
MPD	20.3 ± 2.5	18.2 ± 3.0	0.07
PEG-NH_2	26.0 ± 3.3	26.9 ± 2.0	0.06
perfluorooctyl amine	19.4 ± 2.1	18.0 ± 2.0	0.03

3. Results and discussion

3.1. Surface chemistry of polyamide tuned by termination reactions

Using mLbL, we prepared three replicate films on silicon substrates for subsequent functionalization reactions. Each sample was diced into two pieces: one piece labeled as "as-cast" and one piece that would be subsequently functionalized with the selected reagent. Each "as-cast" piece was subjected to the same reaction conditions (solvent + mild heating) as the functionalized piece but without the functionalization reagent. The mLbL process and subsequent functionalization reactions are shown in Fig. 1.

We measured the thickness of each sample series before and after the functionalization reaction using variable angle spectroscopic ellipsometry (VASE), and the results of these measurements are shown in Table 1.

For the small molecule reagents used for functionalization (TMC, MPD, perfluorooctyl amine), the films exhibited a *decrease* in film thickness (≈10%), likely due to either removal of unreacted monomers or further condensation reaction occurring between TMC and MPD at elevated temperature. Recall that the mLbL deposition occurs in the same solvent as the functionalization reaction (toluene) but at room temperature during the spin process. Furthermore, the functionalization reaction occurs at 75 °C for 48 h, compared with 30 s at room temperature for each mLbL step; thus, there is considerably more opportunity for the functionalization reagents to find unreacted groups at the near surface of the film. Conversely, the PEG-NH_2 functionalization led to a net *increase* in thickness (≈3%) as expected, due to the tethering of a short polymer chain onto the surface. This increase in thickness might be greater if we consider the possible decrease in thickness observed for the small molecular reagents (≈10%). Therefore, the increase in thickness for PEG-NH_2 functionalization might be closer to ≈13%.

Surface functionalization of the mLbL surface was confirmed by XPS. Survey scans of each sample were used to determine the atomic percentage (at%) of each element (C, O, N) in the sample. The O/N ratio is typically taken as a proxy for crosslink density in these polyamide-based membranes: a fully crosslinked polyamide membrane would exhibit an O/N ratio of 1, while a linear polyamide membrane would exhibit an O/N ratio of 2 (the extra oxygen coming from the unreacted –COOH) [35,36]. The O/N ratio data for the mLbL polyamide samples are presented in Table 2. For films reacted with an excess of TMC, we observed an increase in the O/N ratio as more –COOH groups were added to the membrane. This result suggests there are dangling (unreacted) amines at or near the surface that can further react with excess TMC (increasing oxygen content), thus increasing the observed O/N ratio. Conversely, when the film was reacted with an excess of MPD, the O/N decreased considerably as more –NH_2 groups were added via incorporation of more MPD. Surfaces reacted with PEG-NH_2 saw a considerable increase in the O/N ratio as expected, due to the surface being enriched with PEG chains. For the case of surfaces reacted with perfluorooctyl amine, the O/N ratio remained unchanged as the incorporation of the fluorinated chain did not alter the content of either O or N within the film.

Further evidence that the surface functionalization reactions were successful was attained through XPS measurements of the surfaces before and after functionalization. Fig. 2a shows the high-resolution C 1s region of the as-cast TMC-MPD 45.5 cycle mLbL film. Peak fitting clearly showed the presence of C–C/C═C bonds from the aromatic rings of TMC-MPD and/or adventitious carbon (285.0 eV), C–N/C–O bonds from the carbons nearest the amide (285.7 eV), C(=O)N from the amide group (288.4 eV), and C(=O)OH from unreacted acid chlorides in the mLbL film that convert to carboxylic acids upon exposure to moisture (289.4 eV). There is also a small shake-up peak arising from the $\pi \rightarrow \pi^*$ transition of the aromatic rings (291.1 eV). Reacting the surface with an excess of TMC led to a relative increase in the C(=O)O signal in the C 1s region, as shown in Fig. 2b. This is indicative of TMC reacting with any residual –NH_2 groups remaining in the system, placing –COOH groups at the surface. Reacting the surface with an excess of MPD led to the disappearance of the C(=O)O peaks in the C 1s region (Fig. 2c), as any unreacted acid chloride groups were converted to amide bonds, leaving the surface populated by excess aromatic –NH_2 groups. Similarly, when reacting the mLbL surface with excess PEG-NH_2, the residual acid chlorides reacted with the PEG-NH_2, which led to the near disappearance of C(=O)O peak and a concomitant increase in the C–O peak due to the inclusion of PEG, as shown in Fig. 2d. The relatively small C(=O)O peak that remained in the C 1s region is likely due to acid chlorides in the interior of the film that remain inaccessible to the larger reactant PEG-NH_2, as compared with MPD. Finally, reacting the surface with perfluorooctyl amine led to a near disappearance of the C(=O)O peak while giving rise to a C–F peak at 292 eV from the perfluorooctyl group (Fig. 2e). These XPS data confirm in more detail the functionalization of the mLbL film surface with the various reactants.

Table 2
O/N ratio data obtained from XPS survey scans for each sample series before and after functionalization with the specific reagent. The error bars represent one standard deviation of the data (n = 9, measurements at three random locations on each of the three replicate samples), which is taken as the experimental uncertainty of the measurement.

reagent	O/N ratio		
	as-cast	after reaction	percent change
TMC	1.45 ± 0.03	1.80 ± 0.08	+24%
MPD	1.57 ± 0.18	0.88 ± 0.11	−44%
PEG-NH_2	1.71 ± 0.17	3.05 ± 0.59	+78%
Perfluorooctyl amine	1.46 ± 0.10	1.46 ± 0.07	0%

3.2. Effect of terminating monomer on roughness and wetting properties of polyamide

We characterized the surface morphology of the polyamide surfaces using AFM imaging (Fig. 3). All surfaces showed smooth surfaces with a root-mean-square (RMS) roughness of less than 1 nm. This indicates that changing the terminating functional group did not noticeably influence the surface morphology of the polyamide films. The smooth surfaces of the polyamide films are attributed to the controlled polymerization of monomer layers and the stoichiometry-limiting nature of the mLbL method [15]. All the mLbL polyamide films were much smoother than the interfacially polymerized polyamide in RO membrane, which has roughness on the order of 100 nm due to the formation of the "ridge--and-valley" structures during uncontrolled polymerization [9].

We further characterized the surface wetting properties of the polyamide films using the contact angle titration technique pioneered by Whitesides and co-workers [37,38]. A droplet of buffered aqueous solution was placed on the sample surface, and the static contact angle was determined after the droplet and the surface came to equilibrium (Fig. 4). Across the pH range of 2–10 employed here, the perfluorooctyl amine and the PEG-NH_2 functionalized surfaces had the highest and lowest contact angles, respectively, among all surfaces, clearly demonstrating that the wetting properties of the mLbL polyamide surfaces can be readily controlled by using terminating groups with hydrophobic ($-CF_2$) or hydrophilic (PEG) groups. Additionally, the MPD reacted surface had a lower contact angle than the as-cast polyamide surface, consistent with the conversion of residue acid chloride groups to amide bonds and excess polar amine groups as observed in XPS characterization (Fig. 2c).

Buffered contact angle titration measurements also provide information on the near-surface ionization behaviors of the mLbL polyamide films. For the as-cast and TMC-terminated films, the contact angle decreased with increasing pH. This observed trend in contact angle is due to the dominance of carboxyl groups on the film and the changing ionization of carboxyl at different pH [37,39]. Carboxylic acid groups dissociate at low pH. The ionized carboxylate interacts with water more strongly than the undissociated carboxylic acid. The apparent pKa, which characterizes the overall ionization behavior of a surface, on the carboxyl-rich side of interfacially polymerized polyamide was determined to be between 6 and 9 [25], consistent with the pH range of contact angle transition observed in Fig. 4.

For polyamide film terminated with MPD and PEG-NH_2, the pH buffered contact angles exhibit no clear trends, and many of the contact angle values are statistically indistinguishable over the pH range plotted (Fig. 4). Both MPD- and PEG–NH_2–terminated films were rich in amine groups (see Fig. 2 for XPS data), which are more hydrophilic at low pH in their ionized, positively charged state. The apparent pKa of the amine-rich side of interfacially polymerized polyamide was determined to be between 4 and 11, and the exact value varies with charge density [25]. The fact that no clear trend of buffered contact angle was observed implies that MPD and PEG-NH_2 functionalized polyamide films contained a mixture of carboxyl and amine groups. We note that the mLbL

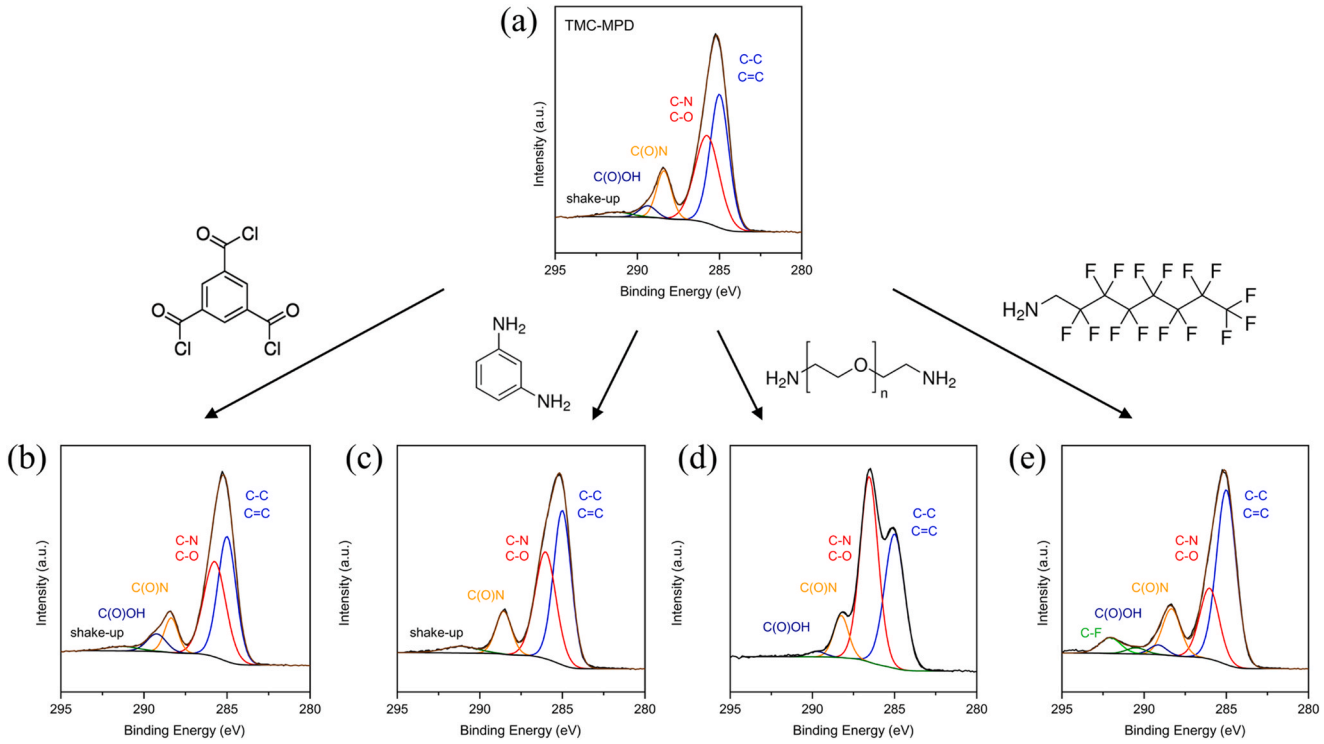

Fig. 2. High-resolution XPS scans of the C 1s region for each surface functionalization reaction. Peak fitting the C 1s envelop shows the appearance, disappearance, or shift in the various carbons resulting from each reaction. (a) As-cast TMC/MPD 45.5 cycle mLbL film, (b) after reaction with excess TMC, (c) after reaction with excess MPD, (d) after reaction with PEG-NH_2, and (e) after reaction with perfluorooctyl amine.

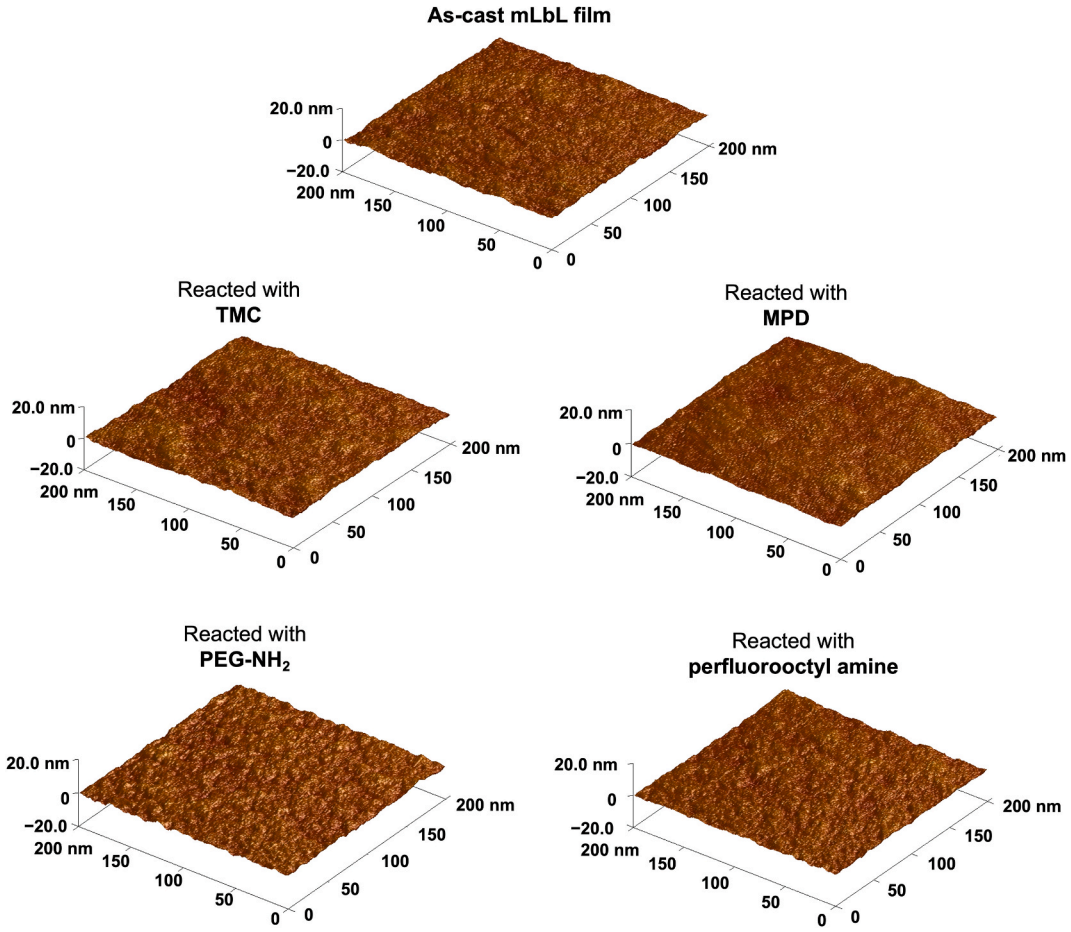

Fig. 3. Three-dimensional AFM images of polyamide films on silicon wafer. The as-cast mLbL film and the films reacted with TMC, MPD, PEG-NH_2, and perfluorooctyl amine have root-mean-square (RMS) roughness of 0.6 ± 0.1, 0.8 ± 0.1, 0.6 ± 0.1, 0.7 ± 0.1, and 0.6 ± 0.1, respectively.

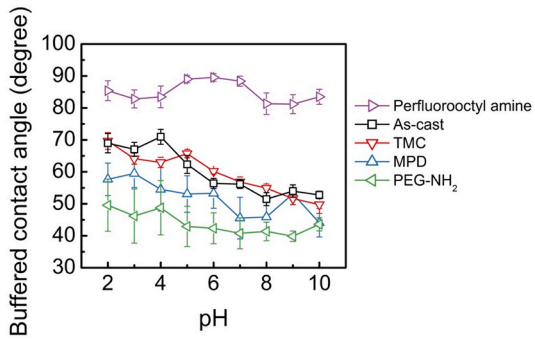

Fig. 4. Buffered contact angle titration of mLbL polyamide films. The error bars represent one standard deviations of the data (n = 3), which is taken as the experimental uncertainty of the measurement. The lines are meant to guide the eye.

polyamide films swell in water (roughly 10%) [17,18]; as a result, the probe liquid likely encounters not only the terminating functional groups, but also functional groups underneath the top layer.

3.3. Effect of terminating monomer on interaction of polyamide surfaces with carboxylate-modified latex (CML) colloidal probe in aqueous solutions

We further conducted AFM force measurements between the polyamide films and a CML-modified AFM probe in a buffered solution of pH 7.5 (Fig. 5a). The CML contains carboxyl groups, which are also functional groups in organic foulants including humic acid and alginate. Previous studies have demonstrated a strong correlation of membrane fouling behaviors with the adhesive forces measured between membrane and CML colloidal probe [40,41]. Specifically, a strong adhesive force between the probe and membrane has been related to a greater flux decline in the initial stage of membrane fouling when foulant-membrane interactions dominate [41]. As such, measuring the interaction forces between the mLbL polyamide surfaces with the CML probe can provide insights into the tendency of mLbL polyamide to undergo organic fouling under specific solution conditions when they are used for water filtration membranes.

The representative forces during the approach of the CML probe to the polyamide surfaces show no appreciable difference between varied surface chemistries (Fig. S1). Hence, we focus our discussion on the retract (or pull-off) force curves. The representative retraction force curves (Fig. 5b) show that the CML particle experienced varied levels of attraction when being pulled away from as-cast, MPD-reacted, and perfluorooctyl amine-reacted polyamide surfaces. We collected 50 force curves on each surface and extracted the maximum adhesive force from the force curves. The box plots for the maximum adhesive force are presented in Fig. 5c. The maximum adhesive force on the polyamide surfaces follows the trend of as-cast > MPD-reacted > perfluorooctyl amine-reacted. On TMC- and PEG–NH_2–reacted surfaces, the interaction between the CML colloid probe and the surfaces was dominated by repulsive force (Fig. 5b). We further calculated the total interaction energy between the CML colloid probe and the polyamide by integrating the area between the force curve and the *x*-axis. The total interaction energy is the sum of both the repulsive and attractive interaction energies in each force curve. The results are shown in Fig. 6a as box plots, and in Fig. 6b as histogram plots with positive values indicating repulsion (red bars) and negative values indicating attraction (black bars).

The as-cast mLbL surface manifests notable adhesive interaction with the CML probe, and 98% of the pull-off events had net attractive interaction (Fig. 6b). We attribute this adhesive interaction to the binding between the carboxyl groups on CML and unreacted residue amine groups on the polyamide. After the surface was reacted with MPD, the adhesive force was still appreciable, but the magnitude of the adhesion decreased (Fig. 6a) and 75% of the pull-off events had net attractive interaction (Fig. 6b). This appears to be a puzzle as we expect MPD reaction with the as-cast polyamide to increase the density of the amine groups on the surface and thereby increase adhesion with the CML probe, which has been observed previously [20]. We note that we used a slightly different experimental condition for preparing the mLbL film compared with what Tousley et al. reported [20]. We dried our mLbL films at 75 °C, whereas Tousley et al. annealed the film to 210 °C [20] which might induce additional crosslinking. The greater adhesion observed for the as-cast compared with MPD-reacted polyamide is possibly due to a relatively loose polymer structure in the top layer of the as-cast film, which allows the CML colloid probe to penetrate further into the film and encounter more amine groups. This hypothesis is corroborated by the decrease in thickness of the film after MPD functionalization (Table 1). We further analyzed the rupture distance during the retraction of the CML probe from the as-cast, MPD, and fluorinated films. The as-cast film had higher rupture distance than the films reacted with MPD or perfluorooctyl amine (Fig. S2), again confirming our hypothesis that the as-cast film had a relatively loose structure which allows the polymer chains to be pull away further by the CML probe.

The CML colloid probe experienced attractive interaction when pulled off from the perfluorooctyl amine reacted polyamide surface, and the attraction was weaker than that on the as-cast and MPD-reacted

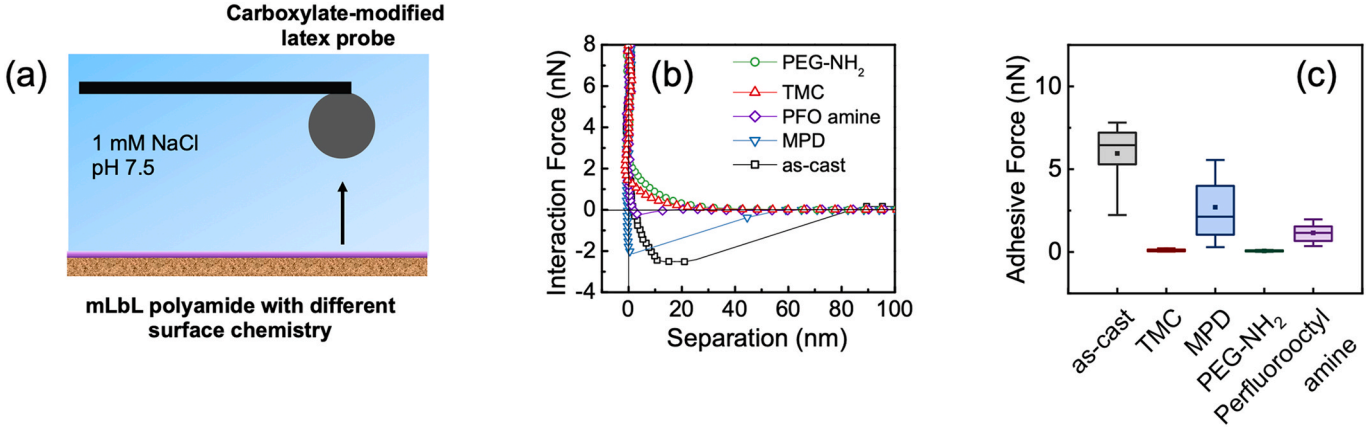

Fig. 5. (a) schematic of AFM force measurement on polyamide surfaces using CML colloid probe. (b) Representative retract forces between the CML colloid probe and mLbL polyamide surfaces as a function of separation distance. PFO amine indicates perfluorooctyl amine. (c) Box plots of the maximum adhesive forces between the CML colloid probe and mLbL polyamide surfaces. Boxes represent 25%, 50%, and 75% quantiles, whiskers represent 10% and 90% quantiles, and dots represent the mean. n = 50.

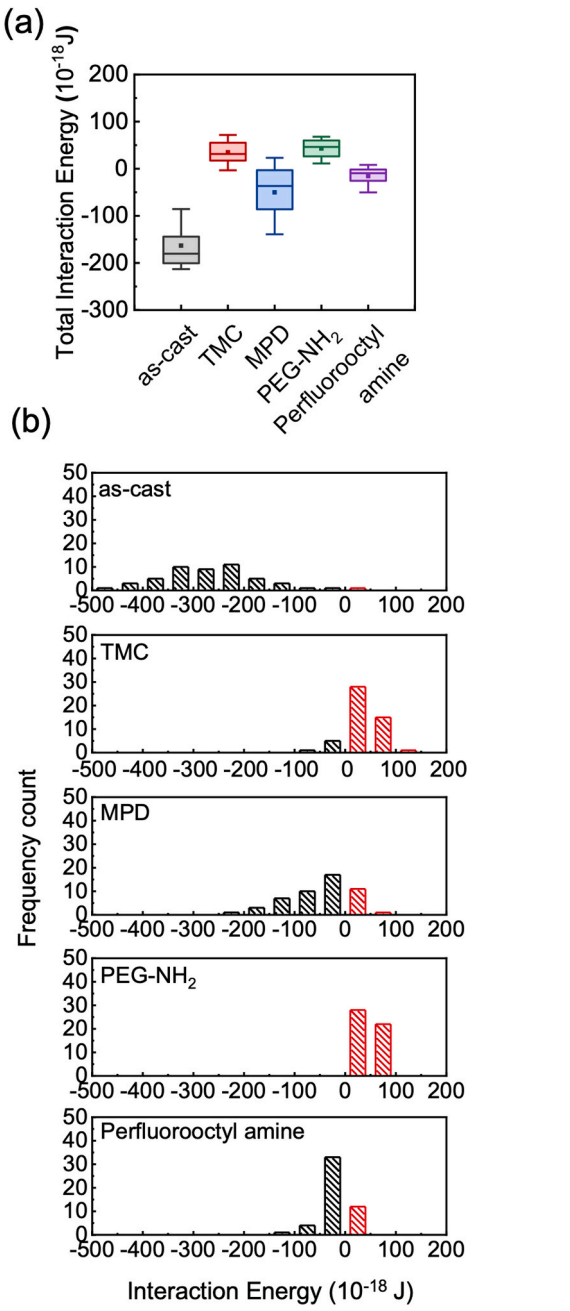

Fig. 6. (a) Box plots of the total interaction energy between the CML colloid probe and the polyamide surfaces calculated from the force curves. n = 50. Boxes represent 25%, 50%, and 75% quantiles, whiskers represent 10% and 90% quantiles, and dots represent the mean. (b) Frequency distribution of total interaction energy. Black bars (negative value) indicate attractive interaction, and red bars (positive value) indicate repulsive interaction. (For interpretation of the references to colour in this figure legend, the reader is referred to the Web version of this article.)

surfaces. We note that functionalizing the as-cast polyamide with perfluorooctyl amine did not reduce the density of amine groups on the surface as evidenced by the unchanged O/N ratio after reaction (Table 2). As such, the reduced adhesion is attributed to the introduction of perfluoroalkyl groups that interact with the CML colloid probe much weaker than the residue amine groups do. Fluorinated materials have low surface free energy [42] and have been employed for fouling-release surfaces due to their weak interaction with foulants [43,44]. Polyamide nanofiltration membranes grafted with perfluoroalkyl groups were reported to show enhanced flux recovery in hydraulic washing following

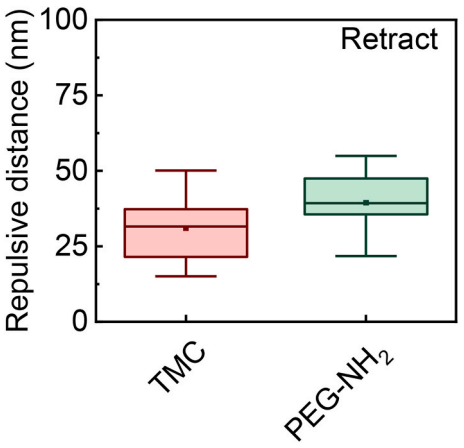

Fig. 7. Box plot of the repulsive distance (nm) of the retract force-distance curves between the CML colloid probe and mLbL polyamide surfaces functionalized by TMC and PEG-NH_2. Repulsive distance is defined as the distance between contact point and the location where repulsive force becomes zero. Boxes represent 25%, 50%, and 75% quantiles, whiskers represent 10% and 90% quantiles, and dots represent the mean. n = 50.

protein fouling [45]. Our AFM force measurements demonstrate the relatively weak interaction between perfluorooctylamine-reacted polyamide and CML probe, which corroborates the promise of fluorinated polyamide in fouling-release filtration membranes.

On the polyamide surfaces reacted with TMC or PEG-NH_2, the retract force-separation curve primarily manifests repulsive interaction. This is expected as these reactions convert the amine groups on the polyamide to –COOH or PEG which have repulsive interactions with the carboxyl groups on the CML colloid probe. The repulsion between TMC-reacted polyamide and CML stems from electrical double layer repulsion between the dissociated carboxyl groups. The repulsion between the CML colloid probe and the PEG–NH_2–reacted polyamide was stronger (Fig. 5b) and extended to longer distance, as indicated by the longer repulsive distance (Fig. 7). Additionally, 100% of the pull-off events had net repulsive interactions (Fig. 6b). This repulsion is likely associated with the steric repulsion that arises when the strongly hydrated PEG chains are compressed by the CML colloid probe [42,46]. Our results show that PEG functionalization of the mLbL polyamide can potentially impart excellent resistance to the adhesion of organic foulants.

It is noteworthy that the buffered contact angles of as-cast and TMC-reacted polyamide surfaces were very similar at pH 7.5, but their adhesion with the CML colloid probe was drastically different. This result suggests that surfaces with similar "apparent" hydrophilicity can have very different interactions with organic foulants, and therefore, propensities to undergo fouling. While contact angle characterizes the hydrophilicity of surface functional groups [37], AFM force measurements reveal the chemical interactions between functional groups on the surface and on the colloid probe [40]. The integration of contact angle measurements and AFM force measurements, therefore, will help gain a full understanding of the fouling propensity of surfaces.

4. Conclusions

We demonstrated here a robust methodology for functionalizing the surface of mLbL polyamide-based membranes. The mLbL process was conducted in such a way as to leave the surface rich in reactive acyl chlorides, which can readily react with various functional amines. Specifically, we reacted the mLbL surface with excess TMC, MPD, amine-terminated PEG, and fluoroalkyl amine, rendering surfaces rich in –COOH, –NH_2, –PEG, and –fluorinated groups. XPS and ellipsometry confirmed successful surface modification while AFM imaging verified that the low surface roughness of each film was maintained. We then

showed that contact angle titration alone cannot adequately capture the surface interactions afforded by each termination chemistry, likely due to the interaction volume of the water droplet on the surface, especially in a system that swells slightly in water. Therefore, AFM colloidal probe measurements with a negatively charged carboxylated latex sphere were performed to gain a clearer picture of the types of surface interactions that might occur during membrane fouling. The measured adhesive interactions display a ranking of $-NH_2 \gg -$fluorinated $>$ $-$COOH $\approx -$PEG. The PEG surface had the strongest repulsive interactions with the carboxylated colloid probe among all surfaces.

Previous studies have shown that polyamide membranes prepared via mLbL deposition (similar to the as-cast polyamide in our work) exhibit superior antifouling performance compared with the interfacially polymerized polyamide, due to the reduced surface roughness and higher chemical homogeneity of the mLbL polyamide [15]. Our work expands the library of the mLbL polyamide surface chemistry by reacting the as-cast film with monomers that have specific functional groups and opens the door to fabricating mLbL polyamide membranes with further enhanced antifouling performance. It also remains to be investigated how changing the surface functionalization impacts the separation performance of the polyamide membranes in water purification applications. As researchers embrace alternative membrane fabrication techniques (atomic layer deposition [47], 3D printing [48], and layered interfacial polymerization [49]), the surface modification schemes demonstrated in this study become more feasible in an effort to tune the surface properties of the resulting membranes.

Finally, our work employs an AFM probe with carboxylic acid groups to quantitatively measure interfacial interactions between two surfaces – the mLbL polyamide and a mimic of model foulants with negative charges. Future work will focus on hydrophobic probes (such as polyethylene) [50] that will provide additional insights into the interactions between polyamide and foulants with hydrophobic domains.

CRediT authorship contribution statement

Christopher M. Stafford: Conceptualization, Methodology, Investigation, Visualization, Writing – original draft, Writing – review & editing. **Xun Guan:** Investigation, Visualization, Writing – review & editing. **Yarong Qi:** Investigation, Visualization, Writing – review & editing. **Yue Zhang:** Formal analysis, Writing – review & editing. **Xitong Liu:** Conceptualization, Methodology, Funding acquisition, Writing – original draft, Writing – review & editing.

Declaration of competing interest

The authors declare that they have no known competing financial interests or personal relationships that could have appeared to influence the work reported in this paper.

Data availability

Data will be made available on request.

Acknowledgments

We acknowledge the support from the start-up funds that X.L. received from the Department of Civil and Environmental Engineering at George Washington University (GW), a Cross Disciplinary Research Fund of X.L. at GW, and the National Science Foundation (CBET 2143508). We thank Dr. Stephen Boyes (GW) for providing access to contact angle goniometer. We are also grateful to Wenjing Shi (GW) for obtaining preliminary data for this project.

Appendix A. Supplementary data

Supplementary data to this article can be found online at https://doi.org/10.1016/j.memsci.2022.120855.

References

[1] M.S. Mauter, I. Zucker, F. Perreault, J.R. Werber, J.H. Kim, M. Elimelech, The role of nanotechnology in tackling global water challenges, Nat. Sustain. 1 (2018) 166–175, https://doi.org/10.1038/s41893-018-0046-8.
[2] M. Elimelech, W.A. Phillip, The future of seawater desalination: energy, technology, and the environment, Science 333 (2011) 712–717, https://doi.org/10.1126/science.1200488.
[3] M.A. Shannon, P.W. Bohn, M. Elimelech, J.G. Georgiadis, B.J. Marinas, A. M. Mayes, Science and technology for water purification in the coming decades, Nature 452 (2008) 301–310, https://doi.org/10.1038/nature06599.
[4] L.F. Greenlee, D.F. Lawler, B.D. Freeman, B. Marrot, P. Moulin, Reverse osmosis desalination: water sources, technology, and today's challenges, Water Res. 43 (2009) 2317–2348, https://doi.org/10.1016/j.watres.2009.03.010.
[5] R. Larson, J. Cadotte, R. Petersen, The FT-30 seawater reverse osmosis membrane–element test results, Desalination 38 (1981) 473–483, https://doi.org/10.1016/S0011-9164(00)86092-0.
[6] J. Cadotte, R. King, R. Majerle, R. Petersen, Interfacial synthesis in the preparation of reverse osmosis membranes, J. Macromol. Sci.-Chem. 15 (1981) 727–755, https://doi.org/10.1080/00222338108056764.
[7] R. Baker, Membrane Technology and Applications, second ed., John Wiley & Sons, 2004.
[8] V. Freger, Nanoscale heterogeneity of polyamide membranes formed by interfacial polymerization, Langmuir 19 (2003) 4791–4797, https://doi.org/10.1021/la020920q.
[9] X.H. Ma, Z.K. Yao, Z. Yang, H. Guo, Z.L. Xu, C.Y.Y. Tang, M. Elimelech, Nanofoaming of polyamide desalination membranes to tune permeability and selectivity, Environ. Sci. Technol. Lett. 5 (2018) 123–130, https://doi.org/10.1021/acs.estlett.8b00016.
[10] M. Elimelech, X.H. Zhu, A.E. Childress, S.K. Hong, Role of membrane surface morphology in colloidal fouling of cellulose acetate and composite aromatic polyamide reverse osmosis membranes, J. Membr. Sci. 127 (1997) 101–109, https://doi.org/10.1016/S0376-7388(96)00351-1.
[11] C. Shang, D. Pranantyo, S. Zhang, Understanding the roughness-fouling relationship in reverse osmosis: mechanism and implications, Environ. Sci. Technol. 54 (2020) 5288–5296, https://doi.org/10.1021/acs.est.0c00535.
[12] P.M. Johnson, J. Yoon, J.Y. Kelly, J.A. Howarter, C.M. Stafford, Molecular layer-by-layer deposition of highly crosslinked polyamide films, J. Polym. Sci., Polym. Phys. Ed. 50 (2012) 168–173, https://doi.org/10.1002/polb.23002.
[13] C. Stafford, P. Johnson, Multi-layer Separation Membrane Formed by Molecular Layer-By-Layer Deposition of Highly Cross-Linked Polyamide Films, 2012. U.S. Patent.
[14] W. Choi, J.E. Gu, S.H. Park, S. Kim, J. Bang, K.Y. Baek, B. Park, J.S. Lee, E.P. Chan, J.H. Lee, Tailor-made polyamide membranes for water desalination, ACS Nano 9 (2015) 345–355, https://doi.org/10.1021/nn505318v.
[15] J.E. Gu, S. Lee, C.M. Stafford, J.S. Lee, W. Choi, B.Y. Kim, K.Y. Baek, E.P. Chan, J. Y. Chung, J. Bang, J.H. Lee, Molecular layer-by-layer assembled thin-film composite membranes for water desalination, Adv. Mater. 25 (2013) 4778–4782, https://doi.org/10.1002/adma.201302030.
[16] W.D. Mulhearn, V.P. Oleshko, C.M. Stafford, Thickness-dependent permeance of molecular layer-by-layer polyamide membranes, J. Membr. Sci. 618 (2021), 118637, https://doi.org/10.1016/j.memsci.2020.118637.
[17] E.P. Chan, S.C. Lee, Thickness-dependent swelling of molecular layer-by-layer polyamide nanomembranes, J. Polym. Sci., Polym. Phys. Ed. 55 (2017) 412–417, https://doi.org/10.1002/polb.24285.
[18] E.P. Chan, A.P. Young, J.H. Lee, C.M. Stafford, Swelling of ultrathin molecular layer-by-layer polyamide water desalination membranes, J. Polym. Sci., Polym. Phys. Ed. 51 (2013) 1647–1655, https://doi.org/10.1002/polb.23380.
[19] D.L. Shaffer, K.E. Feldman, E.P. Chan, G.R. Stafford, C.M. Stafford, Characterizing salt permeability in polyamide desalination membranes using electrochemical impedance spectroscopy, J. Membr. Sci. 583 (2019) 248–257, https://doi.org/10.1016/j.memsci.2019.04.062.
[20] M.E. Tousley, D.L. Shaffer, J.H. Lee, C.O. Osuji, M. Elimelech, Effect of final monomer deposition steps on molecular layer-by-layer polyamide surface properties, Langmuir 32 (2016) 10815–10823, https://doi.org/10.1021/acs.langmuir.6b02746.
[21] D. Rana, T. Matsuura, Surface modifications for antifouling membranes, Chem. Rev. 110 (2010) 2448–2471, https://doi.org/10.1021/cr800208y.
[22] Y. Mo, A. Tiraferri, N.Y. Yip, A. Adout, X. Huang, M. Elimelech, Improved antifouling properties of polyamide nanofiltration membranes by reducing the density of surface carboxyl groups, Environ. Sci. Technol. 46 (2012) 13253–13261, https://doi.org/10.1021/es303673p.
[23] J.R. Werber, C.O. Osuji, M. Elimelech, Materials for next-generation desalination and water purification membranes, Nat. Rev. Mater. 1 (2016), https://doi.org/10.1038/natrevmats.2016.18.
[24] E.P. Chan, J.H. Lee, J.Y. Chung, C.M. Stafford, An automated spin-assisted approach for molecular layer-by-layer assembly of crosslinked polymer thin films, Rev. Sci. Instrum. 83 (2012), 114102, https://doi.org/10.1063/1.4767289.
[25] C.C. Wamser, M.I. Gilbert, Detection of surface functional-group asymmetry in interfacially-polymerized films by contact-angle titrations, Langmuir 8 (1992) 1608–1614, https://doi.org/10.1021/la00042a019.

[26] Q.L. Li, M. Elimelech, Organic fouling and chemical cleaning of nanofiltration membranes: measurements and mechanisms, Environ. Sci. Technol. 38 (2004) 4683–4693, https://doi.org/10.1021/es0354162.
[27] L. Tang, W.Y. Gu, P. Yi, J.L. Bitter, J.Y. Hong, D.H. Fairbrother, K.L. Chen, Bacterial anti-adhesive properties of polysulfone membranes modified with polyelectrolyte multilayers, J. Membr. Sci. 446 (2013) 201–211, https://doi.org/10.1016/j.memsci.2013.06.031.
[28] J.L. Hutter, J. Bechhoefer, Calibration of atomic-force microscope tips, Rev. Sci. Instrum. 64 (1993) 1868–1873, https://doi.org/10.1063/1.1143970.
[29] Y. Zhang, C.C. Wayner, S. Wu, X. Liu, W.P. Ball, S.P. Preheim, Effect of strain-specific biofilm properties on the retention of colloids in saturated porous media under conditions of stormwater biofiltration, Environ. Sci. Technol. 55 (2021) 2585–2596, https://doi.org/10.1021/acs.est.0c06177.
[30] W.A. Ducker, T.J. Senden, R.M. Pashley, Measurement of forces in liquids using a force microscope, Langmuir 8 (1992) 1831–1836, https://doi.org/10.1021/La00043a024.
[31] G. Francius, D. Alsteens, V. Dupres, S. Lebeer, S. De Keersmaecker, J. Vanderleyden, H.J. Gruber, Y.F. Dufrene, Stretching polysaccharides on live cells using single molecule force spectroscopy, Nat. Protoc. 4 (2009) 939–946, https://doi.org/10.1038/nprot.2009.65.
[32] X. Liu, Interactions of silver nanoparticles formed in situ on AFM tips with supported lipid bilayers, Langmuir 34 (2018) 10774–10781, https://doi.org/10.1021/acs.langmuir.8b01545.
[33] B.X. Mi, M. Elimelech, Gypsum scaling and cleaning in forward osmosis: measurements and mechanisms, Environ. Sci. Technol. 44 (2010) 2022–2028, https://doi.org/10.1021/es903623r.
[34] R. Pericet-Camara, G. Papastavrou, S.H. Behrens, C.A. Helm, M. Borkovec, Interaction forces and molecular adhesion between pre-adsorbed poly(ethylene imine) layers, J. Colloid Interface Sci. 296 (2006) 496–506, https://doi.org/10.1016/j.jcis.2005.09.033.
[35] C.Y.Y. Tang, Y.N. Kwon, J.O. Leckie, Probing the nano- and micro-scales of reverse osmosis membranes - a comprehensive characterization of physiochemical properties of uncoated and coated membranes by XPS, TEM, ATR-FTIR, and streaming potential measurements, J. Membr. Sci. 287 (2007) 146–156, https://doi.org/10.1016/j.memsci.2006.10.038.
[36] O. Akin, F. Temelli, Probing the hydrophobicity of commercial reverse osmosis membranes produced by interfacial polymerization using contact angle, XPS, FTIR, FE-SEM and AFM, Desalination 278 (2011) 387–396, https://doi.org/10.1016/j.desal.2011.05.053.
[37] S.R. Holmesfarley, C.D. Bain, G.M. Whitesides, Wetting of functionalized polyethylene film having ionizable organic-acids and bases at the polymer water interface - relations between functional-group polarity, extent of ionization, and contact-angle with water, Langmuir 4 (1988) 921–937, https://doi.org/10.1021/la00082a025.
[38] S.R. Holmesfarley, R.H. Reamey, T.J. Mccarthy, J. Deutch, G.M. Whitesides, Acid-base behavior of carboxylic-acid groups covalently attached at the surface of polyethylene - the usefulness of contact-angle in following the ionization of surface functionality, Langmuir 1 (1985) 725–740, https://doi.org/10.1021/la00066a016.
[39] G. Hurwitz, G.R. Guillen, E.M.V. Hoek, Probing polyamide membrane surface charge, zeta potential, wettability, and hydrophilicity with contact angle measurements, J. Membr. Sci. 349 (2010) 349–357, https://doi.org/10.1016/j.memsci.2009.11.063.
[40] B. Mi, M. Elimelech, Organic fouling of forward osmosis membranes: Fouling reversibility and cleaning without chemical reagents, J. Membr. Sci. 348 (2010) 337–345, https://doi.org/10.1016/j.memsci.2009.11.021.
[41] L. Wang, R. Miao, X. Wang, Y. Lv, X. Meng, Y. Yang, D. Huang, L. Feng, Z. Liu, K. Ju, Fouling behavior of typical organic foulants in polyvinylidene fluoride ultrafiltration membranes: characterization from microforces, Environ. Sci. Technol. 47 (2013) 3708–3714, https://doi.org/10.1021/es4004119.
[42] C.J. Van Oss, Interfacial Forces in Aqueous Media, CRC press, 2006, https://doi.org/10.1201/9781420015768.
[43] S. Krishnan, N. Wang, C.K. Ober, J.A. Finlay, M.E. Callow, J.A. Callow, A. Hexemer, K.E. Sohn, E.J. Kramer, D.A. Fischer, Comparison of the fouling release properties of hydrophobic fluorinated and hydrophilic PEGylated block copolymer surfaces: attachment strength of the diatom Navicula and the green alga Ulva, Biomacromolecules 7 (2006) 1449–1462, https://doi.org/10.1021/bm0509826.
[44] M. Lejars, A. Margaillan, C. Bressy, Fouling release coatings: a nontoxic alternative to biocidal antifouling coatings, Chem. Rev. 112 (2012) 4347–4390, https://doi.org/10.1021/cr200350v.
[45] Y.F. Li, Y.L. Su, X.T. Zhao, R.N. Zhang, J.J. Zhao, X.C. Fan, Z.Y. Jiang, Surface fluorination of polyamide nanofiltration membrane for enhanced antifouling property, J. Membr. Sci. 455 (2014) 15–23, https://doi.org/10.1016/j.memsci.2013.12.060.
[46] J.N. Israelachvili, Intermolecular and Surface Forces: Revised, third ed., Academic press, 2011.
[47] S. Xiong, X. Qian, Z. Zhong, Y. Wang, Atomic layer deposition for membrane modification, functionalization and preparation: a review, J. Membr. Sci. (2022), https://doi.org/10.1016/j.memsci.2022.120740, 120740.
[48] M.R. Chowdhury, J. Steffes, B.D. Huey, J.R. McCutcheon, 3D printed polyamide membranes for desalination, Science 361 (2018) 682–685, https://doi.org/10.1126/science.aar2122.
[49] W. Choi, S. Jeon, S.J. Kwon, H. Park, Y.I. Park, S.E. Nam, P.S. Lee, J.S. Lee, J. Choi, S. Hong, E.P. Chan, J.H. Lee, Thin film composite reverse osmosis membranes prepared via layered interfacial polymerization, J. Membr. Sci. 527 (2017) 121–128, https://doi.org/10.1016/j.memsci.2016.12.066.
[50] T. Horseman, Z. Wang, S. Lin, Colloidal interactions between model foulants and engineered surfaces: interplay between roughness and surface energy, Chem. Eng. J. Adv. 8 (2021), 100138, https://doi.org/10.1016/j.ceja.2021.100138.